

# Practical Pathways to Higher Energy Density LMFP Battery Cathodes

Published as a part of *Energy & Fuels* special issue "2025 Pioneers in Energy Research: Prashant Kamat".

Gerard Bree,\* Jingyi Zhao, Veronika Majherova, Daniela Proprentner, Galo J. Paez Fajardo, and Louis F. J. Piper\*



Cite This: *Energy Fuels* 2025, 39, 3683–3689



Read Online

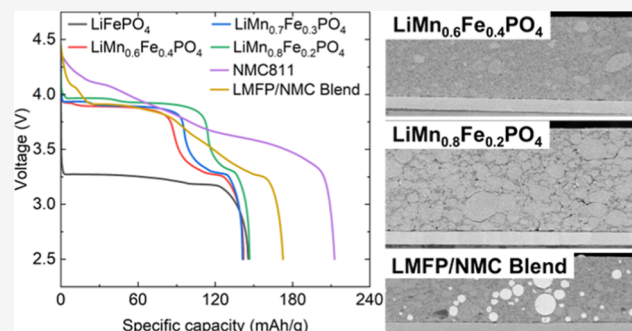
ACCESS |

Metrics & More

Article Recommendations

Supporting Information

**ABSTRACT:** The design of new lithium-ion battery cathode materials must balance many factors: performance, cost, manufacturability, safety, critical mineral usage, and geopolitical constraints. Recently, commercialized  $\text{LiMn}_x\text{Fe}_{1-x}\text{PO}_4$  (LMFP) materials offer good energy density and stability, low material cost, and excellent safety characteristics, avoiding the use of Co or Ni. Within this material set lies a wide variety of potential formulations (Mn/Fe ratio) exhibiting varied cathode properties and challenges. In this work, we assessed three commercially available LMFP materials with Mn content in the range of 60–80% in full cell format, confirming the role of the Mn/Fe ratio on specific capacity, energy density, and electrochemical stability. High Mn content increased the average discharge voltage while maintaining specific discharge capacity, with 80% Mn providing an 18% boost to initial gravimetric energy density over LFP. However, worse kinetics and increased capacity fade rate resulted in the reduction and eventual elimination of this energy density advantage after 100 cycles. A blend cathode (LMFP and  $\text{LiNi}_{0.8}\text{Mn}_{0.1}\text{Co}_{0.1}\text{O}_2$ , NMC811) was also evaluated, exhibiting characteristics of both material types. An initial 23% boost to energy density over LMFP alone was diluted following NMC-dominated degradation in early cycles, but enhanced capacity retention over NMC811 alone remained in long-term cycling. This work highlights the potential advantages of these newly commercialized materials while identifying outstanding challenges to widespread adoption and exploitation.



## INTRODUCTION

The requirement for new lithium-ion battery (LIB) systems exhibiting higher levels of performance continues apace, amid widespread adoption of electric vehicles (EVs), portable electronics, and stationary energy storage systems. Since their introduction in the early 1990s, the energy density of a typical LIB cell has increased from  $\sim 150 \text{ W h kg}^{-1}$  to in excess of  $250 \text{ W h kg}^{-1}$ , all while cost has fallen by up to 97%.<sup>1</sup> This commendable progress has been enabled through a number of achievements: economies of scale and the establishing of efficient vertically integrated supply chains, improvements to cell engineering/design and manufacturing, and the development of higher capacity and lower cost active materials.<sup>2,3</sup> On the cathode side, in particular, the industry has moved from lithium cobalt oxide (LCO,  $\sim 140 \text{ mA h g}^{-1}$ ) to  $\text{LiNi}_{0.33}\text{Mn}_{0.33}\text{Co}_{0.33}\text{O}_2$  (NMC111,  $\sim 160 \text{ mA h g}^{-1}$ ) to  $\text{LiNi}_{0.8}\text{Mn}_{0.1}\text{Co}_{0.1}\text{O}_2$  (NMC811,  $\sim 200 \text{ mA h g}^{-1}$ ).<sup>4</sup> Olivine phosphate materials (such as  $\text{LiFePO}_4$ , LFP with  $170 \text{ mA h g}^{-1}$ ) have also been widely studied academically and adopted commercially, particularly for applications which value low-cost, high safety, and long lifetime. They had historically, however, been unable to compete with NMC layered oxides in terms of energy density, and thus their impact within the

rapidly growing EV sector was secondary.<sup>5</sup> This paradigm has been broken in recent years due to impressive developments in cell and system design, whereby cell/automotive manufacturers (such as BYD) have taken advantage of the excellent safety characteristics of phosphate cathodes (high thermal runaway temperature) to adopt a “cell-to-pack” design strategy.<sup>6</sup> With this approach, assembling large cells directly into a pack without the use of an intermediate module stage, the relative quantity of “inactive” components within the battery system are reduced, enabling greater levels of system-level energy density.<sup>7,8</sup> Additionally, the lower risk of LFP cell rupture/explosion and propagation compared with NMC further reduces the need for inactive packaging.<sup>9</sup> Thus, the energy density gap between layered oxides and phosphate systems has narrowed significantly, which has given rise to a renaissance in phosphate usage over the last 5 years.<sup>10</sup>

Received: December 18, 2024

Revised: January 17, 2025

Accepted: February 4, 2025

Published: February 8, 2025



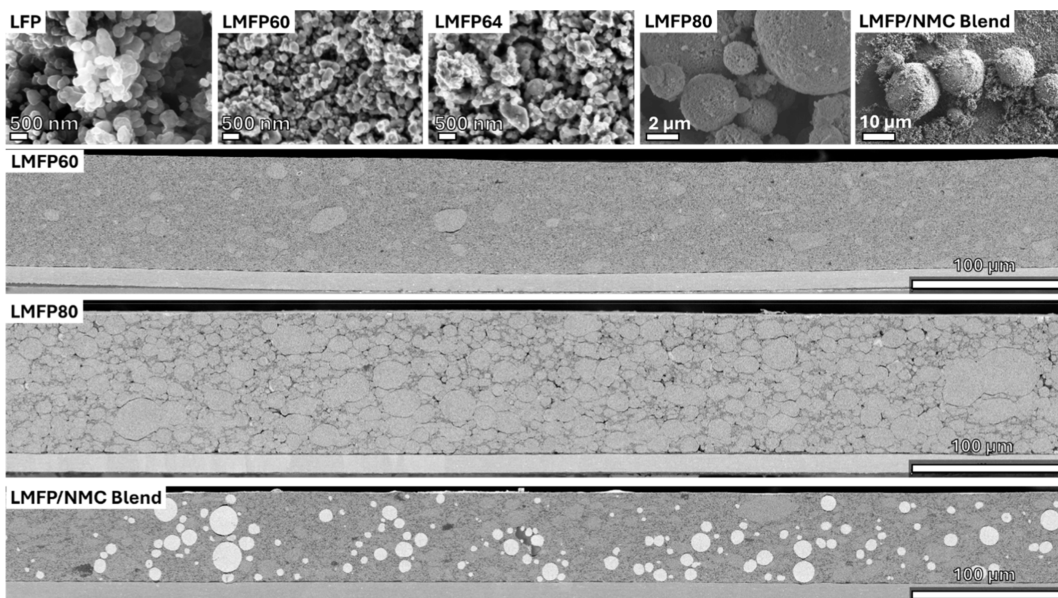


**Figure 1.** SEM images of LFP, LMFP60, LMFP64, LMFP80, and LMFP/NMC blend powders. Cross-sectional SEM images of LMFP60, LMFP80, and LMFP/NMC blend electrodes.

Alongside these engineering developments is the emergence of new LMFP materials, in which some of the Fe in LFP is replaced with Mn, providing greater energy density through the higher oxidation potential of the  $Mn^{2+/3+}$  redox couple.<sup>11,12</sup> However, this advantage comes at a cost. Higher Mn content reduces electrode kinetics due to poor ionic and electronic conductivity associated with Jahn–Teller and polaron distortions.<sup>13–16</sup> Additionally, the cell lifetime can be shortened through Mn disproportionation and dissolution.<sup>17</sup> Thus, there exists a balance between the potential energy density gains from higher Mn content and the greater stability and fast charging capability offered by higher Fe content. LMFP has begun to be adopted in the commercial space, with manufacturers such as CATL and Gotion announcing LMFP (or LMFP-like) batteries.<sup>18,19</sup> More recently, blends of LMFP and NMC have emerged as potential candidates to further bridge the energy density gap between olivines and layered oxides.<sup>20,21</sup> Blending of cathode materials has been widely studied in the academic sphere, utilizing a variety of combinations, notably  $LiNi_{0.5}Mn_{1.5}O_4/LFP$ ,<sup>22</sup>  $LiMn_2O_4/NMC$ ,<sup>23</sup> and  $LMFP/LiNi_{0.85}Co_{0.1}Al_{0.05}O_2$ ,<sup>24</sup> with benefits to cell lifetime, rate capability, and thermal stability identified. In the case of LMFP/NMC blends, a “best of both worlds” is hypothesized, whereby the material can benefit from the higher energy density of NMC while maintaining the good safety characteristics and cell-to-pack efficiency of LMFP. Synergistic buffering effects enabling faster charging have also been highlighted.<sup>25,26</sup> These blends benefit from the compatibility of similar discharge potentials of the two materials ( $\sim 3$ –4.2 V). Thus, a new taxonomy of cathode materials is coming online with virtually infinite variations (Mn/Fe and NMC/LMFP ratios), for which the key performance metrics have not yet been well-defined or understood. The advantages and disadvantages of each necessitate the optimization of cathode chemistry for each distinct application, e.g., high Mn content LMFP particularly suited for energy-dense systems, while lower Mn content (or even simply LFP) may be more suited to fast charging use cases.

In this work, we assess the performance and potential of this generation of materials, focusing on high technology readiness level variants by utilizing commercial materials available in relatively large quantities (tens of kgs) and comparing them with current-gen materials. Through electrode manufacture and cell assembly/testing of LMFP materials with a range of Mn/Fe ratios and an LMFP/NMC blend, critical characteristics including capacity, energy density, and stability during repeated cycling are extracted.

## EXPERIMENTAL SECTION

**Slurry Synthesis and Electrode Manufacture.** LMFP materials with Mn contents of 60%, 64%, and 80%, denoted LMFP60, LMFP64, and LMFP80, were procured from Gelon LIB (LMFP60 and LMFP64) and ALEEES (LMFP80). LFP was obtained from Gelon LIB. The elemental composition of these materials was confirmed via X-ray fluorescence (XRF, see details below). NMC811 was purchased from Li-FUN Technologies. Graphite powder (BTR V–H) was purchased from Targray. All powders were processed utilizing optimized protocols developed in-house based on supplier recommendations. Electrodes were produced via slurry mixing (THINKY ARE-250) and casting (ERICHSEN COATMASTER S10). In a typical mixing process, active material and carbon black (Imerys C6S) powders were weighed and mixed with poly(vinylidene fluoride) (PVDF, Solef S130) predissolved in NMP (8 wt %) to the desired ratio. Further NMP was added in stages to achieve the desired solid content and viscosity for the coating step. LFP, LMFP, and blend electrodes utilized a formulation of 93:3.5:3.5 (AM/CB/PVDF) and were cast onto carbon-coated Al foil (Cambridge Energy Solutions), while NMC811 utilized 95.5:2.5:2 and was cast onto pristine Al foil (Avocet). Electrode coat weights were 135 gsm (13.5 mg cm<sup>-2</sup>) for phosphates/blend and 170 gsm for NMC811. The electrodes were dried overnight under a vacuum at 120 °C. Electrodes were calendered to desired densities of 2.4 g cm<sup>-3</sup> (LFP), 2.15 g cm<sup>-3</sup> (LMFP60 & LMFP64), 1.8 g cm<sup>-3</sup> (LMFP80), 2.4 g cm<sup>-3</sup> (LMFP/NMC blend), 3.3 g cm<sup>-3</sup> (NMC811), and 1.5 g cm<sup>-3</sup> (graphite).

Scanning electron microscopy (SEM) imaging was carried out by using a Sigma Zeiss system. Milling of electrodes for cross-sectional imaging was performed by using a Hitachi IM4000plus Broad Beam Ion Miller. Wavelength-dispersive X-ray fluorescence spectroscopy was conducted at the University of Warwick X-ray diffraction Research Technology Platform using a Rigaku Primus IV system

**Table 1. XRF Analysis of Pristine Phosphate Powders**

material	Mn/Fe	Mg (wt %)	Al (ppm)	Si (ppm)	S (ppm)	Ca (ppm)	Ti (ppm)	Zr (ppm)	Nb (ppm)
LFP	N/A			127	123		1165		
LMFP60	60.2:39.7	0.24	135	121	187	216	644	157	863

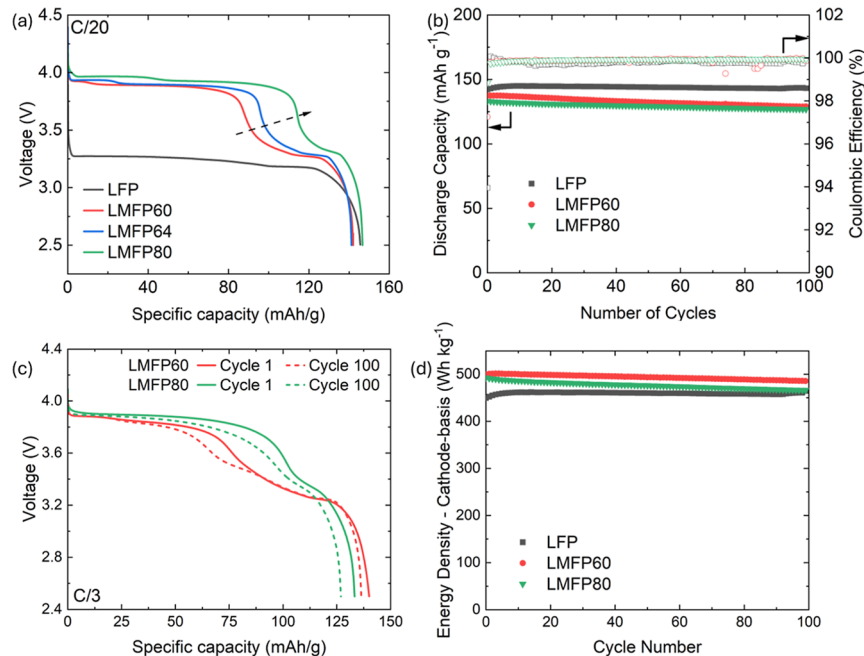


**Figure 2.** (a) Discharge profiles of full phosphate//graphite cells utilizing a range of Mn contents. (b) Performance during C/3 cycling as expressed in terms of gravimetric discharge capacity (with Coulombic efficiency). (c) Voltage profiles of LMFP60 and LMFP80 during the first and 100th discharge. (d) Gravimetric energy density (cathode active material level) during C/3 cycling.

equipped with a 4 kW Rh tube. Elemental compositions were calculated in a semiquantitative manner via the Fundamental Parameters (FP) method using intensity libraries derived from standards analyzed by the instrument manufacturer. SQX is a semiquantitative analysis program utilized here to obtain elemental concentrations without the need for standards by utilizing a theoretical intensity calculation of X-ray intensities using FP and an internal sensitivity library.

**Coin Cell Assembly and Electrochemical Testing.** Discs with diameters of 14.8 mm (cathode) and 15 mm (anode) were punched from the calendered electrode sheets. The graphite anode coat weight was adjusted to achieve NP ratios in the range of 1.1–1.2. 2032 coin cells were assembled in a glovebox with an Argon atmosphere, utilizing 100  $\mu$ L of electrolyte (1 M LiPF<sub>6</sub> in 3:7 EC/EMC + 2% Vinylene Carbonate) and a Celgard 2325 separator. All cell cycling was carried out by using a Biologic BCS cycler coupled with EC-lab software. The cells were allowed to soak for a period of 10 h, after which they underwent a formation process, consisting of two cycles at a rate of C/20. Testing consisted of performing 100 cycles at a rate of C/3, utilizing a constant-current-constant-voltage (CCCV) charging protocol in which the CV stage terminated when current reached C/30. Electrochemical impedance spectroscopy (EIS) was carried out over a frequency range of 10 kHz–10 mHz using a perturbation of 10 mV.

## RESULTS AND DISCUSSION

The range of materials for investigation in this study was chosen to provide insights into the effect of LMFP Mn content on olivine phosphate electrode characteristics, including up to a challenging but advantageous Mn content of 80%. The inclusion of the LMFP/NMC blend material is reflective of recent interest in taking advantage of the unique combined characteristics. To accurately reflect the current industry status,

all materials were commercially obtained and are available in large quantities. First, the morphology of the active materials was studied. The choice of appropriate morphology is heavily dependent on the characteristics of the material in question, with both particle size and crystalline domain size (single-crystal vs polycrystalline) varying with material and manufacturer. Figure 1 shows SEM images of the phosphate and blend cathode material powders examined in this study. Notable is the variation in morphological design strategy undertaken by the material manufacturers. Three of the four nonblend materials exhibited a single-crystalline morphology, with particle size varying from ~100–300 nm (LMFP60/64) to ~500 nm (LFP). The smaller size of LMFP is likely reflective of the reduced ionic conductivity associated with the addition of Mn, necessitating shorter Li diffusion distances. Phosphate materials are typically coated with a thin (<5 nm) carbon layer to further aid electronic conductivity.<sup>27</sup> The outlier here is the LMFP80 material, whereby the manufacturer has elected to arrange the smaller single crystals in porous large secondary particles, maintaining the low required Li<sup>+</sup> diffusion distances and avoiding agglomeration of small crystals during mixing. XRF analysis of the LFP and LMFP60 powders (Table 1) revealed significant Mg content (0.24%) in LMFP60, along with several other dopants such as Ti and Nb, highlighting the adding material complexity necessary when moving from LFP to LMFP. The addition of Mg is widely studied and known to enhance Li<sup>+</sup> diffusion through the mitigation of the Jahn–Teller effect, while Nb can improve particle morphology and electronic conductivity.<sup>28,29</sup> The

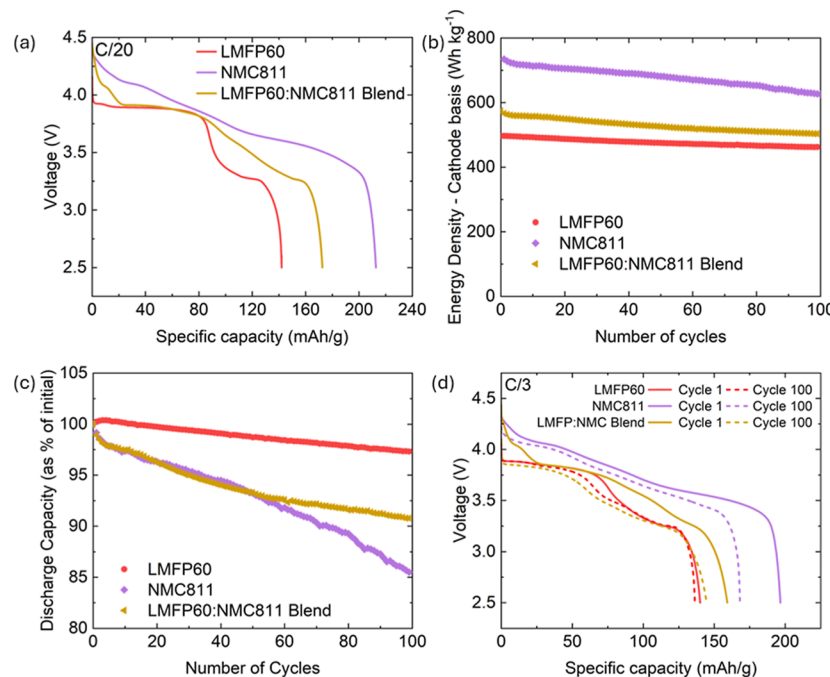


**Figure 3.** (a) Discharge profiles (C/20) and repeated cycling at C/3 of cells produced with LMFP60 and NMC811, along with the blended cathode, expressed as (b) gravimetric energy density (cathode active mass basis) and (c) capacity as a % of initial. (d) Discharge profiles for the first and last C/3 cycle.

LMFP/NMC blend material consisted of a mixture of large 10–20 μm polycrystalline NMC811 particles and LMFP60.

Electrodes were manufactured to a coat weight of 135 gsm (13.5 mg cm<sup>-2</sup>) and calendered to densities of 2.15 g cm<sup>-3</sup> (LFP, LMFP60, and LMFP64), 1.8 cm<sup>-3</sup> (LMFP80), and 2.4 g cm<sup>-3</sup> (LMFP/NMC blend). Cross-sectional imaging of the electrodes (Figure 1) revealed layers approximately 60–90 μm thick. The LMFP60 electrode consisted of LMFP particles largely well dispersed with carbon black, although some larger agglomerates of ~10 μm were visible (higher magnification image shown in Figure S1). Achieving desirable high densities with LMFP80 was more difficult, with cracking/delamination occurring when the density was increased beyond ~1.8 g cm<sup>-3</sup>. This was attributed to the presence of pores within the large secondary particles (highlighted in Figure S1). The blend electrode consisted of NMC811 particles interspersed with LMFP60. The addition of NMC811 enabled greater electrode density through both the higher material density of NMC811 (4.76 g cm<sup>-3</sup>) compared with LMFP60 (3.48 g cm<sup>-3</sup>),<sup>30</sup> and the bimodal particle size, as the smaller LMFP60 particles pack pores between larger NMC811. EDS mapping of the blend electrode (Figure S2) confirmed that NMC was present solely as large polycrystalline particles dispersed throughout the coating.

Full coin cells (utilizing graphite as anode) were produced using the range of cathode materials. Full cell testing (as opposed to a half-cell) with a suitable N/P ratio is critical in extracting meaningful performance data. First, the effect of Mn content in LMFP was examined. Figure 2a shows the discharge voltage profiles of LFP (i.e., no Mn), along with LMFP of 3 grades (60%, 64%, and 80% Mn), when the cells were discharged at C/20. LFP exhibited a single discharge plateau at around 3.25 V, while the LMFP materials exhibited dual plateaus at 3.9 and 3.3 V (relating to the Mn<sup>2+/3+</sup> and Fe<sup>2+/3+</sup> redox reactions, respectively<sup>31</sup>). While all cathodes provided

roughly the same specific discharge capacity ( $144 \pm 3$  mA h g<sup>-1</sup>), the advantage of the higher Mn content is clear, whereby the upper plateau is extended at the expense of the lower, and the total area under the curve (the discharge energy) is thereby increased. The precise values for specific capacity and gravimetric energy density (material-level, based on cathode active mass) are provided in Figure 4. A Mn content of 80% provided an 18% energy density advantage over LFP.

When assessing the potential of these materials, their stability during repeated charging and discharging is also critical. This was assessed through performing 100 cycles of symmetric charge–discharge at C/3 on selected full cells (Figure 2b). When cycling at this higher rate, the detrimental effect of Mn inclusion on electrode kinetics is evident, and LMFP80 exhibits a lower initial capacity than LFP or LMFP60. LFP showed the greatest capacity retention, exhibiting the highest capacity at both the beginning and end of the testing period. Conversely, LMFP materials showed some capacity loss (2.7% in the case of LMFP60 and 4.8% for LMFP80). The added capacity loss experienced by the LMFP materials over LFP can be attributed to Mn dissolution and the resultant poisoning of the anode.<sup>32</sup> Analysis of the energy density decay is, in fact, more meaningful here, as it will also account for any reduction in average discharge voltage brought about by growing heterogeneity and/or polarization in the LMFP cathodes. This voltage decay is visible when discharge profiles for cycle 1 and cycle 100 are examined (Figure 2c), whereby the average discharge voltage of LMFP60 decays from 3.58 to 3.56 V, and that of LMFP80 decays from 3.71 to 3.68 V. Notably, no shift in charge plateau position, which may have indicated increased polarization and impedance were the source of the voltage decay, was observed for LMFP60 (Figure S3a). Consistent with this were the EIS results, whereby the impedance of both cell types was, in fact, lower after 100 cycles compared with that of pristine (Figure S3b). Rather, the decay

in discharge voltages was attributed to a growing heterogeneity within the LMFP electrode.<sup>33</sup> When energy density retention is thus considered (Figure 2d), the initial advantage of the LMFP materials (~10%) begins to decay immediately, and surprisingly, after 100 cycles, the energy density of LFP has matched that of LMFP80. While the benefit of Mn inclusion is clear, it is necessary to improve both the electrode kinetics and cycling stability of these materials to provide a compelling alternative. This result also highlights the importance of calculating and presenting energy density data, as a key degradation mechanism (the voltage decay) is obscured when specific capacity alone is considered.

A cathode blend material, consisting of 70% w/w LMFP60 and 30% NMC811, was similarly examined for its potential. Also included in testing were cathodes consisting of single active materials LMFP60 and NMC811 for reference. Figure 3a shows voltage profiles when full cells (utilizing graphite as anode) were discharged at C/20. The pure LMFP60 cell exhibited a dual plateau as above, while the pure NMC cell exhibited a more gradual slope from ~4.4 to 3.3 V. The voltage profile of the blend material exhibited some characteristics of both its constituents, i.e., activity >4 V (from NMC), a plateau at 3.9 V (from LMFP), and a specific capacity of 173 mA h g<sup>-1</sup>, lying between that of LMFP60 (142 mA h g<sup>-1</sup>) and NMC811 (213 mA h g<sup>-1</sup>). The blend material exhibited a slightly higher average discharge voltage (3.67 V; Figure S4) than LMFP60 (3.64 V), which, when combined with the excess capacity, provided a boost to gravimetric energy density of 23% (Figure 3b). Given the higher true density of NMC (4.7 g cm<sup>-3</sup>) vs LMFP60 (3.6 g cm<sup>-3</sup>), the advantage to volumetric energy density was even more significant at 50%. The inclusion of some NMC also alters the shape of the voltage profile to a more gradual evolution with SOC, beneficial for the determination of state-of-charge (SOC) based on OCV measurement (compared with LMFP alone).<sup>34</sup>

The cells were subjected to repeated cycling to assess the material stability (Figure 3b). Both NMC and the blend material maintained an energy density advantage over LMFP throughout 100 cycles. However, LMFP exhibited the greatest stability, maintaining 93% of initial energy density, while NMC811 fell to 85.3% of initial. Here, both the NMC811 and blend were cycled to an upper cutoff voltage (UCV) of 4.4 V, which, while providing high initial performance, induces oxygen loss and the formation of a reduced surface layer on NMC.<sup>35</sup> This value of UCV was chosen so as to ensure that all LMFP delithiation activity was encompassed and to align with studies of LMFP in the literature.<sup>36,37</sup> The blend material exhibited a capacity loss between that of the unblended variants, maintaining 87.7% of initial energy after 100 cycles. Notably, during the first 55 cycles, the stability trend of the blend material followed that of NMC811 (Figure 3c) but deviated significantly thereafter (absolute capacity and Coulombic efficiency are shown in Figure S5). Degradation mechanisms can be further diagnosed via the analysis of the evolution of discharge voltage profiles during cycling (Figure 3d). Initially, the C/3 profiles look similar to those measured at C/20. However, at the 100th cycle, noticeable changes in profile shape are visible. First, the profile of the NMC811 cell has been depressed due to polarization, attributed to the buildup of a kinetically limiting reduced surface layer on the NMC particles.<sup>38</sup> This is consistent with the obtained EIS spectra (Figure S5c), whereby the impedance of the pure NMC and blend cathodes had evolved and increased

significantly after 100 cycles, but that of the LMFP60 cell had fallen slightly. Second, the blend profile lost many of its NMC-like characteristics, e.g., activity >4.0 V, and instead followed the curve of LMFP60 closely at cycle 100. This reflects the varying rates and modes of degradation of the two materials when combined and poses a challenge to model, predict, and mitigate performance loss behaviors of blend materials.

Figure 4 summarizes the performance (specific capacity and gravimetric and volumetric energy densities) provided by all

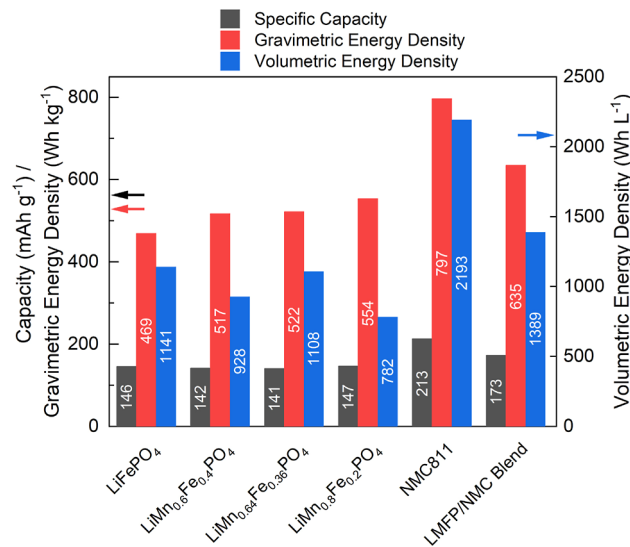


**Figure 4.** Comparison of the specific capacity, gravimetric (cathode active mass basis), and volumetric (cathode active layer basis) energy density for all materials assessed in this study.

cathode materials in the full coin cell format. This data was taken from the second slow formation cycle and thus represents the real potential of these materials if challenges highlighted in this report (poor kinetics/capacity retention) can be mitigated. Increasing the Mn content in LiMn<sub>x</sub>Fe<sub>1-x</sub>PO<sub>4</sub> materials is a clear method of achieving improved gravimetric energy density (18.1% observed in this work) via elevated average discharge voltages; however, further material optimization (via doping, morphological control) is needed to replicate the superior kinetics and stability of LFP. The addition of a small amount of NMC to LMFP materials can further increase gravimetric energy density (at the price of increased manufacturing complexity/cost); however, the challenge of extending cathode stability at high levels of delithiation remains. Furthermore, the addition of NMC may be expected to negatively influence the safety characteristics of the cell, given its lower thermal runaway temperature and higher reaction heat generation.<sup>20,39</sup>

The trend in volumetric density was more nuanced as it considers the material density (g cm<sup>-3</sup>) as well as densification characteristics. Despite the similar material density of 3.6 g cm<sup>-3</sup>,<sup>40</sup> the electrode-level density was lower for LMFP materials (e.g., 2.15 g cm<sup>-3</sup> for LMFP60) than LFP (2.4 g cm<sup>-3</sup>), as suggested by material suppliers. A lower optimum density for LMFP materials likely reflects its poor Li<sup>+</sup> diffusion kinetics and the resultant need for high porosity/low tortuosity. Thus, the volumetric density of LFP was higher than all LMFP materials. LMFP80 in particular exhibited a low maximum electrode density of 1.8 g cm<sup>-3</sup>, above which the

coating cracked and delaminated, and its volumetric energy density was the lowest among all materials studied. The high material density ( $>4.7 \text{ g cm}^{-3}$ <sup>41</sup>) and electrode density ( $3.3 \text{ g cm}^{-3}$ ) of NMC811 is clearly reflected in the volumetric energy density, where it showed a large advantage over phosphate materials. This highlights both a challenge with new LMFP materials and a further benefit from the incorporation of NMC in the blend.

Adjustment of the NMC/LMFP ratio could be expected to achieve specific cell characteristics tuned for particular applications. For example, EVs favor high energy density, and thus, a higher proportion of NMC would likely be optimal, with a smaller content of LMFP to aid with stability and safety. Conversely, stationary energy storage systems prioritize cost/reliability and thus may favor high LMFP content. A true “best of both worlds” blend material would involve optimization of the ratio to capitalize on the high energy density of NMC while maintaining safety characteristics (e.g., thermal runaway temperature) similar to phosphate-only cells, thus enabling the construction of large cell formats and superior system-level energy density.

## CONCLUSIONS

Recent years have seen dramatic increases in the use of phosphate-based cathode materials in EV applications. In this work, several such materials were assessed for specific capacity, energy density, and cycling stability. The addition of Mn to LFP, forming LMFP variants, provided a significant boost to energy density (up to 18% at a Mn content of 80%) associated with a higher average discharge potential, at the cost of poorer electrode kinetics and increased capacity loss during extended cycling. These issues were exacerbated at higher Mn content levels and thus remain as challenges to realizing the full potential of LMFP materials. While further reducing the LMFP active material particle size would be expected to overcome kinetic issues, this poses further challenges with mixing, dispersion, and densification. It thus seems more advantageous to find solutions through material alteration, i.e., doping to enhance diffusion kinetics. Similarly, optimization of electrolyte additives to promote the formation of a stable CEI layer mitigating Mn dissolution is particularly critical at higher Mn content levels.

The combination of LMFP (80% w/w) and NMC811 (20% w/w), forming a blend cathode, provided a 22% capacity and 23% gravimetric energy density advantage over LMFP alone and enabled a greater electrode density, further benefiting volumetric energy density. The emerging use of such blended materials in commercial cells would seem to take advantage of potential synergies, whereby an LMFP-dominated variant with a small amount of NMC (as tested in this work) enables more accurate SOC determination while maintaining a low overall cathode material cost. Conversely, the addition of a small amount of LMFP to NMC-dominated cathodes may offer safety advantages and thus enable larger cell sizes and cell-to-pack designs with greater energy density. However, as highlighted in this work, the issue associated with high voltage cycling of NMC811, namely, poor capacity retention, remains a challenge.

## ASSOCIATED CONTENT

### Supporting Information

The Supporting Information is available free of charge at <https://pubs.acs.org/doi/10.1021/acs.energyfuels.4c06201>.

Further cross-sectional SEM images of LMFP60, LMFP80, and LMFP/NMC blend electrodes; full voltage profiles of the LMFP60 full cell; EIS spectra of LMFP60 and LMFP80; mean discharge voltage for each cell type; discharge capacity, and Coulombic efficiency and EIS spectra for LMFP60, NMC811, and blend material during cycling (PDF).

## AUTHOR INFORMATION

### Corresponding Authors

Gerard Bree – WMG, *Battery Materials and Cells Group, Energy Innovation Centre, University of Warwick, Coventry CV4 7AL, U.K.; The Faraday Institution, Didcot OX11 ORA, U.K.*; [orcid.org/0000-0002-2936-1083](https://orcid.org/0000-0002-2936-1083); Email: [Louis.piper@warwick.ac.uk](mailto:Louis.piper@warwick.ac.uk)

Louis F. J. Piper – WMG, *Battery Materials and Cells Group, Energy Innovation Centre, University of Warwick, Coventry CV4 7AL, U.K.; The Faraday Institution, Didcot OX11 ORA, U.K.*; [orcid.org/0000-0002-3421-3210](https://orcid.org/0000-0002-3421-3210); Email: [Gerard.bree@warwick.ac.uk](mailto:Gerard.bree@warwick.ac.uk)

### Authors

Jingyi Zhao – WMG, *Battery Materials and Cells Group, Energy Innovation Centre, University of Warwick, Coventry CV4 7AL, U.K.*; [orcid.org/0009-0004-3697-543X](https://orcid.org/0009-0004-3697-543X)

Veronika Majherova – WMG, *Battery Materials and Cells Group, Energy Innovation Centre, University of Warwick, Coventry CV4 7AL, U.K.; The Faraday Institution, Didcot OX11 ORA, U.K.*

Daniela Proppertner – WMG, *Battery Materials and Cells Group, Energy Innovation Centre, University of Warwick, Coventry CV4 7AL, U.K.; The Faraday Institution, Didcot OX11 ORA, U.K.*

Galo J. Paez Fajardo – WMG, *Battery Materials and Cells Group, Energy Innovation Centre, University of Warwick, Coventry CV4 7AL, U.K.; The Faraday Institution, Didcot OX11 ORA, U.K.*; [orcid.org/0000-0003-0639-2896](https://orcid.org/0000-0003-0639-2896)

Complete contact information is available at:

<https://pubs.acs.org/10.1021/acs.energyfuels.4c06201>

### Notes

The authors declare no competing financial interest.

## ACKNOWLEDGMENTS

This work was supported by the Faraday Institution [FIRG060 and FIRG062]. The authors would like to acknowledge the contribution of the engineering team in the Energy Innovation Centre and give particular thanks to Hunaynah Abdulgafar for her SEM imaging contributions.

## REFERENCES

- (1) Ziegler, M. S.; Trancik, J. E. Re-examining rates of lithium-ion battery technology improvement and cost decline. *Energy Environ. Sci.* **2021**, *14* (4), 1635–1651.
- (2) Li, J.; et al. Toward Low-Cost, High-Energy Density, and High-Power Density Lithium-Ion Batteries. *JOM* **2017**, *69* (9), 1484–1496.
- (3) Mauler, L.; Duffner, F.; Leker, J. Economies of scale in battery cell manufacturing: The impact of material and process innovations. *Appl. Energy* **2021**, *286*, 116499.
- (4) Liu, J.; Wang, J.; Ni, Y.; Zhang, K.; Cheng, F.; Chen, J. Recent breakthroughs and perspectives of high-energy layered oxide cathode materials for lithium ion batteries. *Mater. Today* **2021**, *43*, 132–165.

- (5) Fichtner, M. Recent Research and Progress in Batteries for Electric Vehicles. *Batteries Supercaps* 2022, 5 (2), No. e202100224.
- (6) Börner, M. F.; et al. Manufacturing cost comparison of tabless vs. standard electrodes for cylindrical lithium-ion batteries. *J. Energy Storage* 2024, 77, 109941.
- (7) Yang, X.-G.; Liu, T.; Wang, C.-Y. Thermally modulated lithium iron phosphate batteries for mass-market electric vehicles. *Nat. Energy* 2021, 6 (2), 176–185.
- (8) Pampel, F.; Pischinger, S.; Teuber, M. A systematic comparison of the packing density of battery cell-to-pack concepts at different degrees of implementation. *Results Eng.* 2022, 13, 100310.
- (9) Schöberl, J.; Ank, M.; Schreiber, M.; Wassiliadis, N.; Lienkamp, M. Thermal runaway propagation in automotive lithium-ion batteries with NMC-811 and LFP cathodes: Safety requirements and impact on system integration. *eTransportation* 2024, 19, 100305.
- (10) IEA. *Global EV Outlook 2024*; International Energy Agency, 2024.
- (11) Padhi, A. K.; Nanjundaswamy, K. S.; Goodenough, J. B. Phospho-olivines as Positive-Electrode Materials for Rechargeable Lithium Batteries. *J. Electrochem. Soc.* 1997, 144 (4), 1188.
- (12) Reed, S.; Scanlan, K.; Manthiram, A. Scalable, low-cost synthesis of high volumetric capacity LiMn0.5Fe0.5PO4 cathode for lithium-ion batteries. *J. Mater. Chem. A* 2024, 12 (32), 21341–21349.
- (13) Lv, Z.; Li, M.; Lin, J.; Luo, J.; Wu, B.; Hong, R.; Cao, S. C. First-principles study on LiMn0.5Fe0.5PO4 doping to decrease the Jahn-Teller effect. *J. Solid State Electrochem.* 2024, 28 (2), 577–587.
- (14) Piper, L. F. J.; et al. Elucidating the Nature of Pseudo Jahn-Teller Distortions in  $\text{Li}_x\text{MnPO}_4$ : Combining Density Functional Theory with Soft and Hard X-ray Spectroscopy. *J. Phys. Chem. C* 2013, 117 (20), 10383–10396.
- (15) Yang, R.; et al. A critical revelation of lithium ferromanganese phosphate (LMFP) performance in a Mn-rich cathode for Li-ion batteries using Fe equivalents to occupy a Mn site. *J. Mater. Chem. C* 2024, 12 (14), 4961–4976.
- (16) Lv, W.; et al. Discovering Cathodic Biocompatibility for Aqueous  $\text{Zn}-\text{MnO}(2)$  Battery: An Integrating Biomass Carbon Strategy. *Nanomicro Lett.* 2024, 16 (1), 109.
- (17) Hu, Q.; et al. High-throughput screening of high energy density  $\text{LiMn}_{1-x}\text{FePO}_4$  via active learning. *Chin. Chem. Lett.* 2025, 36, 110344.
- (18) China's CATL to Start Mass Output of M3P Batteries This Year; Reuters, 2023.
- (19) CleanTechnica. Gotion Introduces LMFP Battery with Energy Density of 240 Wh/kg. <https://cleantechnica.com/2023/05/20/gotion-introduces-lmfp-battery-with-energy-density-of-240-wh/kg/> (accessed Nov 14, 2024).
- (20) Jobst, N. M.; Hoffmann, A.; Klein, A.; Zink, S.; Wohlfahrt-Mehrens, M. Ternary Cathode Blend Electrodes for Environmentally Friendly Lithium-Ion Batteries. *ChemSusChem* 2020, 13 (15), 3928–3936.
- (21) Dahn, J. R.; Yang, C.; Yue, M.; Aiken, C. P. Blended Cathode Active Material Including Iron Phosphate based and Nickel Oxide Based Materials, and Methods Thereof. WO/2024/229047, 2024.
- (22) Versaci, D.; et al. Tailoring cathode materials: A comprehensive study on LNMO/LFP blending for next generation lithium-ion batteries. *J. Power Sources* 2024, 613, 234955.
- (23) Chandra, K. P.; Budarapu, P. R. Design and analysis of Lithium-ion pouch cell with LMO-NMC blended cathode using coupled thermo-electro-chemical model. *J. Energy Storage* 2024, 78, 109958.
- (24) Zhang, B.; et al. Synthesis of flexible LiMn0.8Fe0.2PO4/C microsphere and its synergistic effects with blended LiNi0.85Co0.10Al0.05O2 electrodes. *J. Power Sources* 2022, 541, 231671.
- (25) Heubner, C.; Liebmann, T.; Lämmel, C.; Schneider, M.; Michaelis, A. Synergy Effects in Blended Electrodes for Li-ion Batteries: A Conceptual Clarification. *Batteries Supercaps* 2022, 5 (1), No. e202100171.
- (26) Chatzogiannakis, D.; et al. Towards understanding the functional mechanism and synergistic effects of  $\text{LiMn}_2\text{O}_4$  -  $\text{LiNi}_0.5\text{Mn}_0.3\text{Co}_0.2\text{O}_2$  blended positive electrodes for Lithium-ion batteries. *J. Power Sources* 2024, 591, 233804.
- (27) Wen, L.; et al. Effect of Carbon-Coating on Internal Resistance and Performance of Lithium Iron Phosphate Batteries. *J. Electrochem. Soc.* 2022, 169 (5), 050536.
- (28) Vanaphuti, P.; Manthiram, A. Enhancing the Mn Redox Kinetics of  $\text{LiMn}(0.5)\text{Fe}(0.5)\text{PO}_4(4)$  Cathodes Through a Synergistic Co-Doping with Niobium and Magnesium for Lithium-Ion Batteries. *Small* 2024, 20 (47), No. e2404878.
- (29) Guo, H.; Liu, R.; Li, W.; Gu, H.; Cao, J.; Gong, D.; Liang, G. Site Selection of Niobium-Doped  $\text{LiMn}_0.6\text{Fe}_0.4\text{PO}_4$  and Effect on Electrochemical Properties. *J. Electrochem. Soc.* 2023, 170 (3), 030542.
- (30) Zhang, B.; et al. High-energy-density lithium manganese iron phosphate for lithium-ion batteries: Progresses, challenges, and prospects. *J. Energy Chem.* 2025, 100, 1–17.
- (31) Wi, S.; et al. Insights on the delithiation/lithiation reactions of  $\text{Li}_{x}\text{Mn}_0.8\text{Fe}_0.2\text{PO}_4$  mesocrystals in  $\text{Li}^{+}$  batteries by in situ techniques. *Nano Energy* 2017, 39, 371–379.
- (32) Leslie, K.; Harlow, J.; Rathore, D.; Tuul, K.; Metzger, M. Correlating Mn Dissolution and Capacity Fade in  $\text{LiMn}_0.8\text{Fe}_0.2\text{PO}_4/\text{Graphite}$  Cells During Cycling and Storage at Elevated Temperature. *J. Electrochem. Soc.* 2024, 171 (4), 040520.
- (33) Hu, Q.; Wang, L.; Han, G.; Liao, J.; Liu, J.; Yao, J.; He, X. Revealing the voltage decay of  $\text{LiMn}_0.7\text{Fe}_0.3\text{PO}_4$  cathodes over cycling. *Nano Energy* 2024, 123, 109422.
- (34) Zhang, K.; Xiong, R.; Li, Q.; Chen, C.; Tian, J.; Shen, W. A novel pseudo-open-circuit voltage modeling method for accurate state-of-charge estimation of  $\text{LiFePO}_4$  batteries. *Appl. Energy* 2023, 347, 121406.
- (35) Menon, A. S.; Shah, N.; Gott, J. A.; Fiamegkou, E.; Ogley, M. J. W.; Páez Fajardo, G. J.; Vaenas, N.; Ellis, I.; Ravichandran, N.; Cloetens, P.; et al. Quantifying Electrochemical Degradation in Single-Crystalline  $\text{LiNi}_0.8\text{Mn}_0.1\text{Co}_0.1\text{O}_2$ -Graphite Pouch Cells through Operando X-Ray and Postmortem Investigations. *PRX Energy* 2024, 3 (1), 013004.
- (36) Zhong, Y.-J.; Li, J.-T.; Wu, Z.-G.; Guo, X.-D.; Zhong, B.-H.; Sun, S.-G.  $\text{LiMn}_0.5\text{Fe}_0.5\text{PO}_4$  solid solution materials synthesized by rheological phase reaction and their excellent electrochemical performances as cathode of lithium ion battery. *J. Power Sources* 2013, 234, 217–222.
- (37) Hu, Q.; et al. Ultrahigh rate capability of manganese based olivine cathodes enabled by interfacial electron transport enhancement. *Nano Energy* 2022, 104, 107895.
- (38) Páez Fajardo, G. J.; et al. Synergistic Degradation Mechanism in Single Crystal Ni-Rich NMC//Graphite Cells. *ACS Energy Lett.* 2023, 8 (12), 5025–5031.
- (39) Ouyang, D.; Liu, Y.; Hamam, I.; Wang, J.; Dahn, J. A comparative study on the reactivity of charged Ni-rich and Ni-poor positive electrodes with electrolyte at elevated temperatures using accelerating rate calorimetry. *J. Energy Chem.* 2021, 60, 523–530.
- (40) Wei, X.; Zhang, M.; Miao, B.; Liu, R. Volumetric capacity enhancement in  $\text{LiFePO}_4$  cathodes by hot isostatic pressing. *Scr. Mater.* 2021, 194, 113638.
- (41) Nguyen, T.-T.; Delobel, B.; Berthe, M.; Fleutot, B.; Demortière, A.; Delacourt, C. Mathematical Modeling of Energy-Dense NMC Electrodes: I. Determination of Input Parameters. *J. Electrochem. Soc.* 2022, 169 (4), 040546.